



OPEN ACCESS

EDITED BY

Changxiang Li,
Beijing University of Chinese Medicine, China

REVIEWED BY

Shinya Dohgu,
Fukuoka University, Japan
Vanessa Coelho-Santos,
Coimbra Institute for Biomedical Imaging
and Translational Research (CIBIT), Portugal
Abraham Jacob Al-Ahmad,
Texas Tech University Health Sciences Center,
United States

*CORRESPONDENCE

Tao Wang
✉ tao.wang@manchester.ac.uk

RECEIVED 28 March 2023

ACCEPTED 16 May 2023

PUBLISHED 08 June 2023

CITATION

Zhang W, Zhao X, Qi X, Kimber SJ, Hooper NM
and Wang T (2023) Induced pluripotent stem
cell model revealed impaired neurovascular
interaction in genetic small vessel disease
Cerebral Autosomal Dominant Arteriopathy
with Subcortical Infarcts
and Leukoencephalopathy.
Front. Cell. Neurosci. 17:1195470.
doi: 10.3389/fncel.2023.1195470

COPYRIGHT

© 2023 Zhang, Zhao, Qi, Kimber, Hooper and
Wang. This is an open-access article distributed
under the terms of the [Creative Commons
Attribution License \(CC BY\)](https://creativecommons.org/licenses/by/4.0/). The use,
distribution or reproduction in other forums is
permitted, provided the original author(s) and
the copyright owner(s) are credited and that
the original publication in this journal is cited,
in accordance with accepted academic
practice. No use, distribution or reproduction is
permitted which does not comply with
these terms.

Induced pluripotent stem cell model revealed impaired neurovascular interaction in genetic small vessel disease Cerebral Autosomal Dominant Arteriopathy with Subcortical Infarcts and Leukoencephalopathy

Wenjun Zhang¹, Xiangjun Zhao¹, Xuewei Qi¹, Susan J. Kimber²,
Nigel M. Hooper^{3,4} and Tao Wang^{1,4,5*}

¹Division of Evolution, Infection and Genomic Sciences, School of Biological Sciences, Faculty of Biology, Medicine, and Health, The University of Manchester, Manchester, United Kingdom, ²Division of Cell Matrix Biology and Regenerative Medicine, School of Biological Sciences, Faculty of Biology, Medicine, and Health, The University of Manchester, Manchester, United Kingdom, ³Division of Neuroscience, School of Biological Sciences, Faculty of Biology, Medicine, and Health, The University of Manchester, Manchester, United Kingdom, ⁴Geoffrey Jefferson Brain Research Centre, Manchester Academic Health Science Centre, Northern Care Alliance NHS Group, The University of Manchester, Manchester, United Kingdom, ⁵Manchester Centre for Genomic Medicine, Manchester University NHS Foundation Trust, Manchester, United Kingdom

Introduction: Cerebral Autosomal Dominant Arteriopathy with Subcortical Infarcts and Leukoencephalopathy (CADASIL) is the most common genetic small vessel disease caused by variants in the *NOTCH3* gene. Patients with CADASIL experience recurrent strokes, developing into cognitive defect and vascular dementia. CADASIL is a late-onset vascular condition, but migraine and brain MRI lesions appear in CADASIL patients as early as their teens and twenties, suggesting an abnormal neurovascular interaction at the neurovascular unit (NVU) where microvessels meet the brain parenchyma.

Methods: To understand the molecular mechanisms of CADASIL, we established induced pluripotent stem cell (iPSC) models from CADASIL patients and differentiated the iPSCs into the major NVU cell types including brain microvascular endothelial-like cells (BMECs), vascular mural cells (MCs), astrocytes and cortical projection neurons. We then built an *in vitro* NVU model by co-culturing different neurovascular cell types in Transwells and evaluated the blood brain barrier (BBB) function by measuring transendothelial electrical resistance (TEER).

Results: Results showed that, while the wild-type MCs, astrocytes and neurons could all independently and significantly enhance TEER of the iPSC-BMECs, such capability of MCs from iPSCs of CADASIL patients was significantly impaired. Additionally, the barrier function of the BMECs from CADASIL iPSCs was significantly decreased, accompanied with disorganized tight junctions in iPSC-BMECs, which could not be rescued by the wild-type MCs or sufficiently rescued by the wild-type astrocytes and neurons.

Discussion: Our findings provide new insight into early disease pathologies on the neurovascular interaction and BBB function at the molecular and cellular levels for CADASIL, which helps inform future therapeutic development.

KEYWORDS

CADASIL, genetic small vessel disease, neurovascular interaction, blood-brain barrier, neurovascular unit

1. Introduction

CADASIL (Cerebral Autosomal Dominant Arteriopathy with Subcortical Infarcts and Leukoencephalopathy) is a genetic small vessel disease (SVD) caused by heterozygous variants in the *NOTCH3* gene (Joutel et al., 1996; Sharma et al., 2001). Although a rare condition, CADASIL represents the most common type of monogenic SVD with a prevalence of 2–5 per 100,000 people and a likelihood of being underdiagnosed (Razvi et al., 2005; Narayan et al., 2012; Rutten et al., 2016). Patients with CADASIL usually experience recurrent ischemic strokes, migraines with aura, psychiatric disturbances and seizures, and gradually develop to cognitive impairment and vascular dementia (Joutel et al., 1997; Charlton et al., 2006; Chabriat et al., 2009; Adib-Samii et al., 2010). Despite excellent research carried out in this field, molecular mechanisms underlying this condition are still not entirely clear, therefore, no specific and effective treatments are available to date.

Typical pathological changes observed in CADASIL patients include vascular smooth muscle cell (VSMC) degeneration in small arteries, accumulation of the extracellular domain of NOTCH3 protein, deposition of granular osmiophilic materials (GOM) around VSMCs, and thickening of small blood vessel walls (Joutel et al., 1997, 2001; Chabriat et al., 2020). However, the mechanisms by which vascular dysfunction leads to clinical manifestations in the brain has not been fully understood. Recurrent strokes in CADASIL patients would certainly damage brain function, contributing to the development of cognitive defects and the eventual dementia. However, CADASIL is a late-onset condition where strokes usually occur between 40 and 50 years of age. According to the natural history of CADASIL patients, migraine with aura and abnormalities of white matter on T2 weighted MRI images happen as early as in their teens and twenties, well before the onset of strokes (Desmond et al., 1999; Chabriat et al., 2009). This suggests a likelihood of defects at the interface where blood vessels meet the brain parenchyma.

In the central nervous system (CNS), functional connections between blood vessels and neurons rely on a unique structure—the neurovascular unit (NVU) comprising mainly brain microvascular endothelial cells (BMECs), mural cells (MCs, including pericytes on capillaries and VSMCs on arterioles), astrocytes, and neurons. BMECs are surrounded by MCs that are embedded in the basement membrane, and the microvessels are ensheathed by astrocyte endfeet that bridge to the neurons and are surrounded by microglia (Andreone et al., 2015). Complex and dynamic interactions between these neurovascular cell types regulate the blood-brain barrier (BBB) function and cerebral blood flow (CBF), which helps to maintain the homeostasis of the CNS (Abbott et al., 2006;

Daneman and Prat, 2015). Therefore, the NVU, as the neurovascular interface, is a key target for understanding the molecular mechanisms of CADASIL and SVD in general, which could potentially inform future drug development.

The BMECs are the central component of the BBB structure and have unique properties distinct from ECs in peripheral vasculatures. BMECs have a low rate of transcytosis, a lack of fenestrations, and are particularly enriched in tight junction proteins (e.g., claudin-5, occludin, ZO-1) that are essential in reducing paracellular diffusions and contribute to the barrier function of BBB (Coomber and Stewart, 1985; Wallez and Huber, 2008; Daneman and Prat, 2015). BMECs have high numbers of transporters. The glucose transporter (GLUT-1) is critically important for brain function by maintaining the continuous glucose level and energy demands to support neural cell growth and activities (Yazdani et al., 2019). The ATP-binding cassette (ABC) efflux transporter family members (e.g., p-glycoprotein) are responsible for eliminating harmful substances from the brain into the blood (Chai et al., 2022). The highly polarized nature of BMECs ensures efficient transportation to occur between the brain and blood. The expression of leukocyte adhesion molecule is also low in BMECs, which greatly limits the entry of peripheral immune cells into the CNS, thus protecting the brain from damage when inflammation occurs (Daneman et al., 2010a; Daneman and Prat, 2015). The tight barrier property of BMECs creates a high trans-endothelial electrical resistance (TEER) of $>1,000 \Omega \cdot \text{cm}^2$, which is commonly measured using a Voltmeter in experimental settings *in vitro* (Neal et al., 2019; Newman et al., 2020). The BBB permeability can also be determined by observing the diffusion of fluorescent small molecules across the BMEC monolayer (Stebbins et al., 2016).

The unique barrier property of BMECs is not intrinsic to the cells but induced by the CNS environment (Janzer and Raff, 1987). Other neurovascular cell types in the NVU significantly strengthen the barrier function of BMECs (Daneman and Prat, 2015; Hongjin et al., 2020). Neural progenitor cells (NPCs) regulate CNS vascularization in the developing brain (Tata and Ruhrberg, 2018), and the neuronal activity is also important in the establishment of the efflux transporters of the BBB (Pulido et al., 2020). Astrocytes enhance the BBB barrier function through their perivascular endfeet and the secretion of a range of soluble factors (Alvarez et al., 2013). Capillaries in the CNS have significantly higher pericyte coverage than the peripheral vascular bed, which contributes to the regulation of the BBB (Brown et al., 2019). However, the functional interactions between the neurovascular cell types have not been addressed in CADASIL at the cellular level. We hypothesized that impairments of the neurovascular

interaction at the NVU contribute to the development of the CADASIL phenotype.

We have previously established induced pluripotent stem cell (iPSC) models from CADASIL patients and demonstrated an intrinsic defect of MCs in supporting angiogenic tubule structures, likely via a downregulation of PDGFR β in MCs and a detrimental effect to the adjacent ECs (Kelleher et al., 2019). This iPSC model was employed in the current study. We differentiated iPSCs into BMEC-like cells (BMECs), astrocytes and cortical projection neurons, in addition to VSMCs and ECs, to uncover the possible damage to neurovascular interactions in CADASIL.

2. Materials and methods

2.1. Cell lines and cell culture

The CADASIL iPSC lines were established from skin biopsies of two CADASIL patients carrying *NOTCH3* variants Arg153C and Cys224Try, respectively, as reported in our previous study (Kelleher et al., 2019). The five control iPSC clones were from three healthy individuals with two iPSC clones (02C3 and 02C9) reported by Kelleher et al. (2019), two clones (SW171a and SW174a) reported by Wood et al. (2020), Woods et al. (2020), and OX1-19 line reported by Jarosz-Griffiths et al. (2019). Prior to differentiation, all iPSCs were cultured in Vitronectin Recombinant Human Protein (VTN-N) (ThermoFisher, A14700, Loughborough, UK) pre-coated six-well plates with 2 mL TeSR-E8 medium (STEMCELL Technologies, 05990, Cambridge, UK) at 37°C with 5% CO₂, except for the OX1-19 iPSCs that were cultured on Matrigel (Corning, 354277, Deeside, UK) pre-coated 6-well plates in mTeSR1 complete medium (STEMCELL Technologies, 85850, Cambridge, UK).

Primary human coronary arterial endothelial cells (HCAECs) (PromoCell, C-12222, Heidelberg, Germany) were cultured in six-well plates (Corning, 3516) with 2 mL Endothelial Cell Growth Medium (MV2, PromoCell, C-22121, Heidelberg, Germany) and maintained at 37°C incubator with 5% CO₂.

2.2. Differentiation of iPSCs into brain microvessel endothelial-like cells (BMECs)

The BMEC differentiation protocol was adapted from Lippmann et al. (2012, 2014). iPSCs were seeded on Matrigel pre-coated six-well plate at a cell density 250,000–400,000 per well in TeSR-E8 medium, termed day 0. From day 0 to day 5 the medium was changed daily with 2 mL DMEM/F-12 containing 20% KnockOut™ Serum Replacement (ThermoFisher, Loughborough, UK), 1 x Non-Essential Amino Acid (NEAA, Life Technologies, 11140, Warrington, UK), 0.5 x L-glutamine and 0.1 mM β -mercaptoethanol. On day 6, the medium was replaced by Human Endothelial serum free medium (hESFM, ThermoFisher, 11111, Loughborough, UK) containing 1% Human Platelet Poor Plasma-derived Serum (HS, Sigma, P2918, Gillingham, UK), 20 ng/mL FGF2 and 10 μ M All-trans Retinoic Acid (RA, Sigma, R2625, Gillingham, UK) and cultured for 2 days. On day 8, BMECs

were sub-cultured onto plates or Transwells that were pre-coated with solution of Collagen IV (1 mg/mL in acetic acid, Sigma, C5533, Gillingham, UK)/fibronectin (Sigma, F1141, Gillingham, UK)/water (C/F/W) to be 4:1:5 for purification of BMECs and measurement of the TEER.

2.3. Differentiation of iPSCs into cortical projection neurons

Induced pluripotent stem cells differentiation into cortical projection neurons was adapted from a protocol by Shi et al. (2012). iPSCs were dissociated with EDTA and seeded on to 12-well plates (Corning) pre-coated with Matrigel and cultured in TeSR-E8 medium. When reaching 100% confluency, the culture medium was changed to neural induction medium (NIM) containing 1 μ M Dorsomorphin (Tocris, 3093, Bristol, UK) and 10 μ M SB431542 (Tocris, 1614, Bristol, UK) in neural maintenance medium (NMM). NMM was a 1:1 mixture of N2 (ThermoFisher, 17502001, Loughborough, UK) and B27 medium (ThermoFisher, 17504044, Loughborough, UK). N2 medium consisted of DMEM/F-12 GlutaMAX medium (Life Technologies, 31331, Warrington, UK), 1 x N2, 5 μ g/mL insulin (Sigma, I9278, Gillingham, UK), 1 mM L-Glutamine (Life Technologies, 25030024, Warrington, UK), 100 μ M NEAA, 100 μ M 2-mercaptoethanol (Life Technologies, 31350, Warrington, UK) and 0.5% Penicillin-Streptomycin (10,000 U/mL) (Life Technologies, 15140, Warrington, UK). B27 medium consists of 1 x Neurobasal medium (Life Technologies, 12348, Warrington, UK), 1 x B27, 200 mM L-Glutamine and 0.5% Penicillin-Streptomycin. The medium was changed daily.

On day 10–12 after induction, the cells were passaged with 0.5 mL Dispase (Life Technologies, 17105, Warrington, UK) and transferred onto Laminin (Sigma, L2020, Gillingham, UK) pre-coated six-well plate and cultured in 2 mL fresh NIM. After 24 h, medium was changed to NMM containing 20 ng/mL Recombinant Human FGF-basic (FGF2) (PeproTech, 100-18C, London, UK) for 3–4 days. FGF2 was then withdrawn when neural rosettes appeared, and cells were maintained in NMM. Rosettes were isolated from cultures using Neural Rosette Selection Reagent (STEMCELL Technologies, 05832, Cambridge, UK), this was the NPC stage.

On day 25 after induction, cells were dissociated into single cells with Accutase (STEMCELL Technologies, 07920, Cambridge, UK) and transferred into a new Laminin pre-coated plate with medium changed every other day. Mature neurons after day 60 were used for all experiments.

2.4. Differentiation of iPSCs into astrocytes

During neuron differentiation, selected neural rosettes were seeded onto Laminin pre-coated six-well plate and cultured with 2 mL of NMM at 37°C for 24 h, this was marked as day 0 of astrocyte differentiation. On day 1, medium was changed to 2 mL of complete STEMdiff™ Astrocyte Differentiation Medium (ADM) (STEMCELL Technologies, 08540, Cambridge, UK). On day 7 and day 14, cells were passaged with Accutase and seeded onto Laminin pre-coated plate at a density of 1×10^5 cells/cm² and

cultured in ADM that was changed every other day. On day 21, cells were passaged and seeded as above and cultured in complete STEMdiff™ Astrocyte Maturation Medium (AMM) (STEMCELL Technologies, 08550, Cambridge, UK) with medium changed every other day. Cells were further passaged on days 28 and 35. After day 35, mature astrocytes were observed.

2.5. Differentiation of iPSCs into mural cells (MCs) and endothelial cells (ECs)

The differentiations of MCs and ECs from iPSCs were described in our previous publication (Kelleher et al., 2019). Briefly, iPSCs were seeded on to VTN-N coated plates. For MC differentiation via neuroectoderm, TeSR-E8 medium was replaced with Essential six medium (E6, Life Technologies, A1516401, Warrington, UK) supplemented with 10 ng/mL FGF2 and 10 μM SB431542. The medium was changed every day until day 8 when medium was replaced by E6 medium supplemented with 10 ng/mL human Platelet-Derived Growth Factor BB (PDGF-BB, PeproTech, 100-14B, London, UK) and 2 ng/mL Recombinant Human Transforming Growth Factor-β1 (TGF-β1, PeproTech, 100-21, London, UK). Cells were passaged when they reached 70% confluency until day 18. For EC differentiation, E8 medium was replaced with E6 medium supplemented with 6 μM CHIR99021 (Tocris Bioscience, 4423, Bristol, UK), 20 ng/mL Bone Morphogenetic Protein 4 (rBMP4, PeproTech, 120-05, London, UK) and 10 ng/mL FGF2 and cultured for 3 days. On day 3, medium was replaced with E6 supplemented with 50 ng/mL vascular endothelial growth factor (VEGF, PeproTech, 100-20, London, UK), 10 ng/mL FGF2 and 20 ng/mL rBMP4, and the medium was changed on day 5. On day 7, cells were cultured in E6 medium supplemented with 50 ng/mL VEGF, 10 ng/mL FGF2 and 10 μM SB431542, and the medium was changed every other day. On day 12, endothelial cells were purified using a CD31 MicroBead Kit (Miltenyi Biotec, 130-091-935, Woking, UK) and further cultured in the Promocell endothelial cell medium (MV2) until use.

2.6. *In vitro* neurovascular unit (NVU) model and TEER measurement

On day 8 of the BMEC differentiation as described in section “2.2 Differentiation of iPSCs into brain microvessel endothelial-like cells (BMECs)” above, the iPSC-BMECs were dissociated using Accutase (Invitrogen, A1110501, ThermoFisher, Loughborough, UK), 1.1×10^6 cells were seeded on to the C/F/W pre-coated 0.4 μm pore diameter 12-well Transwell filter and cultured in the Transwell. From day 9, medium was changed to hESFM medium with 1% HS (without FGF2 and RA), and the TEER was recorded using an Epithelial Volt/Ohm Meter EVOM2™ (EVOM with STX2 electrodes, World Precision Instrument, Hitchin, UK) on days 24, 48, 72, 96, and 120 h after cell seeding. TEER measurements were normalized by subtracting the background and then multiplying by the surface area (1.12 cm²) of the Transwell filter and presented as Ω/cm². All TEER experiments

were performed with at least three triplicate wells, and from at least three independent differentiations.

2.7. Sodium fluorescein permeability assay

Sodium fluorescein permeability was measured as described previously (Stebbins et al., 2016). At day 8 of the BMEC differentiation, cells were cultured onto C/F/W pre-coated Transwells at a density of 1.1×10^6 cells per well of a 12-well Transwell. The permeability coefficient of the cells was indicated as Pe (centimeters per minute). A blank pre-coated Transwell was set up as control to determine the Pe value through the support membrane for each experiment (Blank). Then all medium was removed and pre-warmed hESFM with 1% HS was added to both top chambers (0.5 mL) and bottom wells (1.5 mL). Cells were incubated for 60 min at 37°C, followed by TEER measurement to ensure the starting barrier tightness. Sodium fluorescein salt (F6337, Sigma, Gillingham, UK) was diluted to 10 μM in the same culture medium. Then the medium in the top chamber was removed and replaced with 500 μL of the fluorescein loaded medium, with brief, gentle pipetting. Samples of 150 μL medium from the bottom wells was collected at 15, 30, 45, and 60 min time point, and the missing volume was replaced by adding an equal volume of pre-warmed fresh cell culture medium to the wells. At the 60 min time point, 150 μL medium from each of the top Transwell chambers were also collected (Max). Control samples (Background) consisted of 150 μL of hESFM including 1% HS without sodium fluorescein. The fluorescence of all samples in 96-well plates was measured by a plate reader (Synergy HT platereader, BioTek) using a setting of 485 nm excitation/530 nm emission.

The permeability of sodium fluorescein was analysed according to the method described (Stebbins et al., 2016). First, the signal of the samples at each time point was corrected by removing background ($Sample' = Sample - Background$), and the signal loss from the bottom chamber was also counted [e.g., $30 \text{ min } Sample^{corrected} = 30 \text{ min } Sample' + (15 \text{ min } Sample' * 150 \mu L / 1,500 \mu L)$]. Then the clearance volume at each time point was calculated:

$$Clearance \ volume = (VB * Sample^{corrected}_t) / ST^{Max}$$

Where VB is the volume of bottom chamber (1,500 μL); $Sample^{corrected}_t$ is the corrected signal of bottom chamber at time t; ST^{Max} is the signal of top chamber at 60 min. Afterward the linear slope of clearance volume against time was calculated using linear regression for both Sample (ms) and the Blank filter (mb). The sodium fluorescein permeability (Pe) was calculated using the following formula:

$$1/Pe = 1/ms - 1/mb.$$

$$Pe \ (cm/min) = [(1/(1/Pe))/1,000]/Area.$$

Where Area is the area of the Transwell filter.

2.8. Angiogenesis tubule formation assay

Induced pluripotent stem cell-ECs at day 14 or iPSC-BMECs at day 10 of differentiation were used for the tubule formation assay.

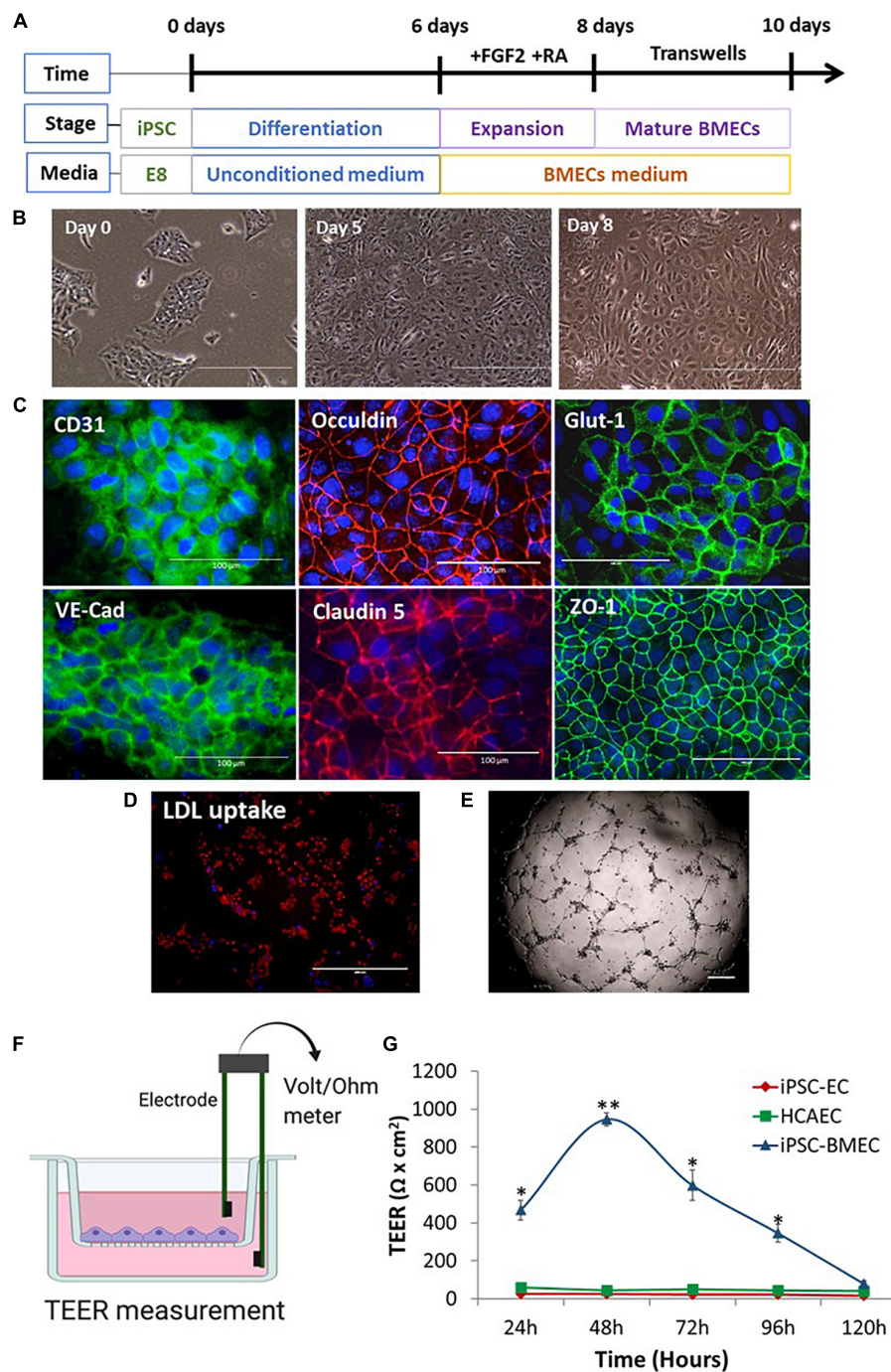


FIGURE 1
Brain microvascular endothelial-like cell (BMEC) differentiation from induced pluripotent stem cells (iPSCs) and characterizations. **(A)** Schematic illustration of BMEC differentiation protocol. **(B)** Morphological changes of iPSC during BMEC differentiation under light microscope. **(C)** Immunofluorescent staining of BMEC marker proteins, including adherence junction proteins (CD31, VE-cadherin), tight junction proteins (Occludin, claudin 5, ZO-1), and glucose transporter, Glut-1. Scale bars, 100 μm . **(D)** iPSC-BMECs at day 10 differentiation were treated with the Dil-ac-low-density lipoproteins (LDL) dye and visualized under fluorescent microscope. Scale bar, 200 μm . **(E)** *In vitro* angiogenesis assay on Matrigel. Scale bar, 200 μm . **(F)** Schematic illustration of the *in vitro* neurovascular unit (NVU) using Transwell setting. The blood-brain barrier (BBB) function is measured as transendothelial electrical resistance (TEER) using a Voltmeter. **(G)** iPSC-BMECs, iPSC-endothelial cells (ECs), and human coronary artery endothelial cells (HCAECs) were seeded on to the insert of the Transwell, respectively. The TEER was measured each day for five consecutive days (120 h). Data are represented as mean \pm SEM, $n = 3$. Two-way ANOVA with Tukey's *post-hoc* test, * $p < 0.05$, ** $p < 0.01$. Figure **(F)** was created using BioRender.

Ten thousand HCAECs, HUVECs, iPSC-ECs or BMECs in 200 μL cell culture medium were plated onto 96-well plates pre-coated with a thin layer of Matrigel (50 μL per well), respectively. HCAECs were

seeded in 200 μL Endothelial Cell Growth Medium MV2. iPSC-ECs were seeded in E6 medium supplemented with 5 ng/mL VEGF-165 and 2 ng/mL FGF2. iPSC-BMECs were seeded in hESFM with

50 ng/mL VEGF-165 without RA or FGF2. Phase-contrast images were acquired at 3, 6, 24, 48, and 72 h of culture in a CO₂ incubator on an EVOS™ XL Core Imaging System microscopy (AMEX1000, ThermoFisher Scientific) using 4x objectives.

2.9. Low density lipoprotein uptake assay

Differentiated BMECs at day 10 were analysed with the Dil-ac-LDL dye (J65597, Alfa Aesar, Heysham, UK). Culture medium was aspirated then incubated in medium containing 12 µg/mL Dil-ac-LDL for 4 h at 37°C, 5% CO₂. Cells were then washed three times with PBS and fixed with 4% paraformaldehyde for 10 min. Images were taken with a fluorescent microscope with an excitation wavelength of 594 nm.

2.10. Calcium wave imaging of astrocytes

At day 100 of the differentiation, the iPSC-derived astrocytes were labeled using 20 µM Ca²⁺ indicator dye Fluo-4 AM (Invitrogen, ThermoFischer, Loughborough, UK) for 30–60 min depending on absorption rate of individual cells until the basal fluorescence of fluo-4 in all cells plateaued to a constant level. Recordings excitation/emission wavelengths 494/506 nm were made by confocal time-lapse microscopy under a Zeiss LSM 880 Biolumi confocal laser scanning microscope with a 40x oil objective (Carl Zeiss, Birmingham, UK). Spontaneous activity of cells was recorded for 10 min. Five random fields were chosen under the microscope and averaged for each sample. Time-lapse recording and images were analysed using Zeiss microscopy software ZEN, MicroExcel and ImageJ.

2.11. Immunofluorescent staining

Immunofluorescent staining was performed as previously described (Wang et al., 2007). Briefly, cells were fixed with 4% paraformaldehyde, permeabilized with 0.2% Triton X-100 for 3–10 min at room temperature and incubated with blocking buffer (10% donkey serum). The cells were then incubated with primary antibodies at appropriate dilutions (Supplementary Table 1) in blocking buffer for 1 h at room temperature or overnight at 4°C, followed by incubating with fluorescent conjugated secondary antibodies (Supplementary Table 1) and counterstained by DAPI. Images were collected on an Olympus BX51 upright microscope using an objective (20x/0.5 UPlan FLN) and captured using a Coolsnap ES2 camera (Photometrics) through Metavue v7.8.4.0 software (Molecular Devices). Images were then processed and analysed using Fiji ImageJ.

2.12. Quantitative real time polymerase chain reaction (qRT-pPCR)

Quantitative real time polymerase chain reaction was carried out according to our previous report (Kelleher et al., 2019). Briefly, Total RNA was extracted from cells using an RNeasy mini kit

(Qiagen, 74104, Manchester, UK) and reverse transcribed into cDNA. QRT-PCR was performed using PowerUp™ SYBR™ Green Master Mix (ThermoFisher, A25742, Loughborough, UK) with PCR cycles of 95°C for 10 min, followed by 40 cycles of 95°C for 15 s and 60°C for 1 min. *GAPDH* was used as endogenous control. Data was analysed using $2^{-\Delta \Delta Ct}$ or the Pfaffl method (Pfaffl, 2001) in which differences in primer efficiencies were accounted for. Primers used in the study are listed in [Supplementary Table 2](#).

2.13. Statistics

Data were presented as mean ± standard error (SEM). GraphPad PRISM was used for data analysis and statistical tests. Comparisons of two groups were made using an unpaired *t*-test. For comparisons of data sets above two samples, one-way or two-way ANOVA with Tukey's multiple comparisons *post-hoc* test was used. The sample size used for statistical analysis came from at least three independent iPSC differentiations from the iPSC lines (biological replicates), and each experiment included three technical repeats.

3. Results

3.1. Neurovascular interactions enhance the barrier function of iPSC-BMECs but mural cells from CADASIL patients fail to enhance these interactions

Brain microvascular endothelial-like cells were differentiated from iPSCs according to published protocols (Lippmann et al., 2012, 2014; [Figure 1A](#)). During differentiation, the iPSCs gradually lost the typical colonized growth nature of stem cells and acquired cobblestone morphology ([Figure 1B](#)). The iPSC-BMECs displayed endothelial markers (CD31 and VE-cadherin), tight junction proteins (occludin, claudin5 and ZO1), as well as the glucose transporter (Glut1) on immunofluorescent staining ([Figure 1C](#)). Functional assays revealed that the iPSC-BMECs had the ability to take up low-density lipoproteins (LDL) ([Figure 1D](#)) and formed vessel network structures when cultured on Matrigel ([Figure 1E](#)). To determine the BBB function, the TEER value was recorded across the iPSC-BMEC monolayer in a Transwell setting ([Figure 1F](#)), which showed a peak TEER ~1,000 Ω·cm². The barrier function of iPSC-BMECs was compared with that of both iPSC-derived peripheral ECs and human coronary artery endothelial cells (HCAECs), which showed that the TEER of iPSC-BMECs was significantly higher than the ECs ([Figure 1G](#)).

We then moved on to determine if our iPSC-derived neurovascular cell types could enhance the barrier function of iPSC-BMECs. MCs were differentiated from iPSCs via the neuroectoderm according to our previous report (Kelleher et al., 2019). Differentiation of astrocytes and cortical projection neurons from iPSCs are shown in [Supplementary Figures 1, 2](#), respectively. The iPSC-BMECs on day 8 of differentiation were seeded on the Transwell insert that was pre-coated with collagen IV and

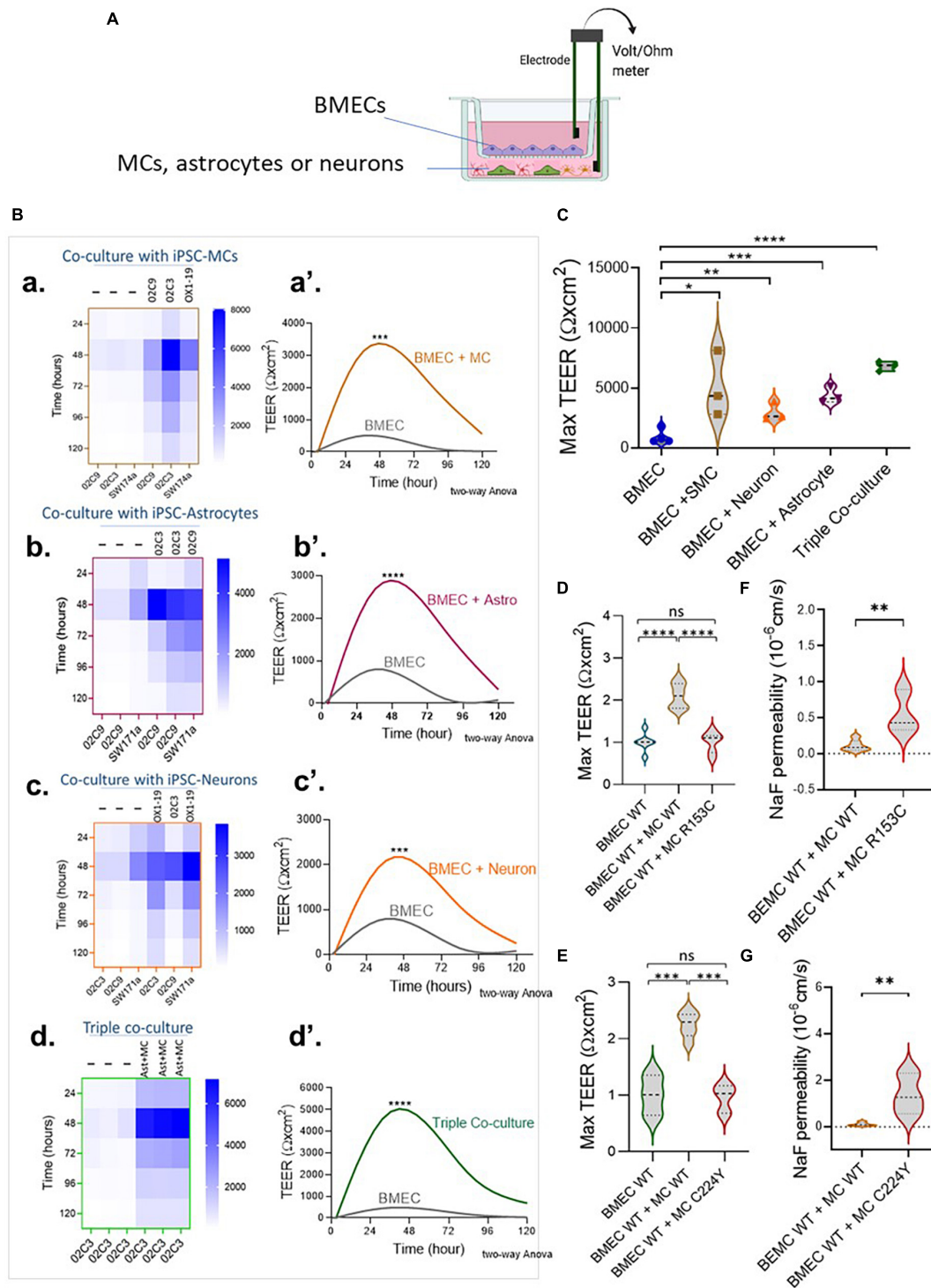


FIGURE 2

The regulation of brain microvascular endothelial-like cell (BMEC) barrier function by induced pluripotent stem cell (iPSC)-derived mural cells (MCs), astrocytes and neurons. **(A)** Schematic illustration of the Transwell co-culture neurovascular unit (NVU) system. **(B)** Wild-type (WT) iPSC-BMECs were seeded on the insert of Transwell and co-cultured with the wild-type (WT) iPSC derived MCs **(a,a')**, astrocytes **(b,b')** and neurons **(c,c')**, as well as both astrocytes and neurons [Triple co-culture, **(d,d')**] that were grown on the bottom of the Transwell plate. Transendothelial electrical resistance (TEER) was measured each day for five consecutive days. **(A,a–d)** Heatmaps represent the raw TEER of independent experiments with or without co-culture. **(A,a'–d')** Fit spline curves demonstrate a trend of differences between the BMECs mono-culture and co-culture groups throughout 120 h. Two-way ANOVA before *post-hoc* test demonstrated an overall difference between the two groups ($***p < 0.001$, $****p < 0.0001$). **(C)** Comparison of maximum TEER between groups presented in **(B)**. **(D,E)** BMECs derived from WT iPSCs were co-cultured with MCs from either WT iPSCs or Cerebral Autosomal Dominant Arteriopathy with Subcortical Infarcts and Leukoencephalopathy (CADASIL) *NOTCH3* variants R153C **(D)** or R224Y **(E)**, and the fold change of maximum TEER were compared. Data are presented as mean \pm SEM, $n = 3$ in **(C,D,E)**, and One-way ANOVA with Tukey's *post-hoc* test, $*p < 0.05$, $**p < 0.01$, $***p < 0.001$, and $****p < 0.0001$, $n = 3$. **(F,G)** BMECs derived from WT iPSCs were co-cultured with MCs from either WT iPSCs or CADASIL *NOTCH3* variants R153C **(F)** or R224Y **(G)**, and sodium fluorescein (NaF) permeability was measured. Data are mean \pm SEM, unpaired *t*-test, $**p < 0.01$, $n = 3$. Figure **(A)** was created using BioRender.

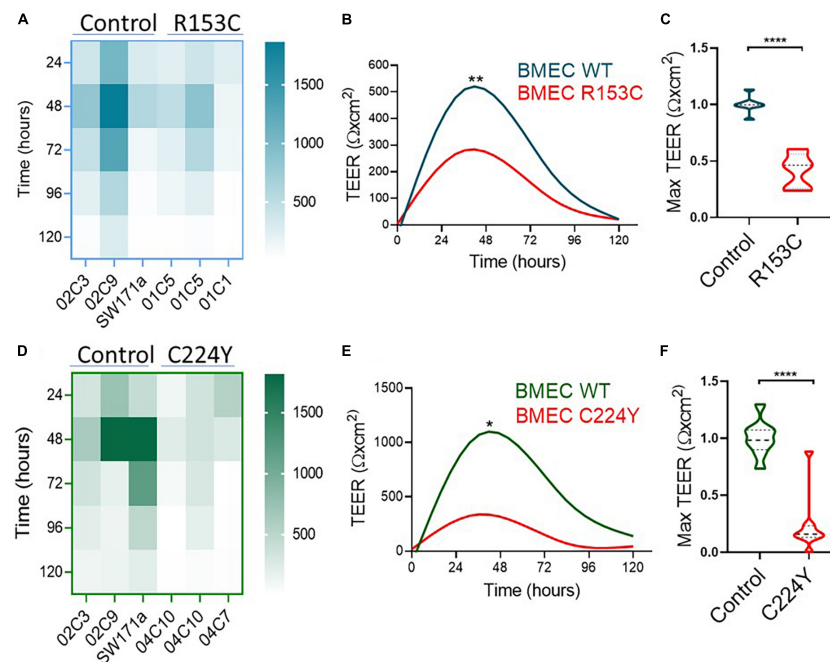


FIGURE 3

Transendothelial electrical resistance (TEER) measurement on brain microvascular endothelial-like cells (BMECs) generated from induced pluripotent stem cells (iPSCs) of Cerebral Autosomal Dominant Arteriopathy with Subcortical Infarcts and Leukoencephalopathy (CADASIL) patients. iPSCs from CADASIL patients carrying *NOTCH3* variants R153C (A–C) or C224Y (D–F) and healthy control individuals were differentiated into BMECs. TEER was measured for five consecutive days (120 h). (A,D) Heatmaps represent the raw TEER of independent experiments for *NOTCH3*^{R153C} (A) and *NOTCH3*^{C224Y} (D). Fit spline curves (B,E) show a trend of difference between the controls (WT) and mutant groups. Two-way ANOVA before *post-hoc* test demonstrated an overall difference between the two groups (**p* < 0.05, ***p* < 0.01). (C,F) The fold changes of maximum TEER were compared between the control and CADASIL patients carrying *NOTCH3* variant R153C (C) and C224Y (F). Data are presented as mean ± SEM. Student's *t*-test, *****p* < 0.0001, *n* = 3.

fibronectin for a further 2 days, which helps to purify the BMECs, and then co-cultured with MCs, astrocytes and neurons that were growing on the bottom of the Transwells (Figure 2A), respectively. The TEER was then measured over five consecutive days. Results showed that iPSC derived MCs, astrocytes and neurons could all significantly enhance the TEER of the iPSC-BMECs (Figures 2B, C). However, MCs from iPSCs of both CADASIL patients carrying *NOTCH3*^{R153C} and *NOTCH3*^{C224Y} both failed to enhance the barrier function of the iPSC-BMECs (Figures 2D, E). This was confirmed by the sodium fluorescein permeability assay (Figures 2F, G).

3.2. The barrier function of BMECs derived from CADASIL iPSCs is impaired

Having validated the functionalities of the iPSC-derived neurovascular cells and their interactions, we went on to determine if the barrier function of BMECs derived from iPSCs of CADASIL patients was impaired. Interestingly, we consistently observed a low TEER of iPSC-BMECs from both CADASIL patients as compared with the controls (Figure 3). This finding is supported by the immunofluorescent staining where the tight junction proteins (Claudin 5 and Occludin) in the iPSC-BMECs from the two CADASIL patients were significantly disorganized compared to the control iPSC-BMECs (Figure 4), although ZO-1 and Glut-1 did not show significant mis-localization (Figure 4).

Considering the fact that *NOTCH3* is generally expressed in the MCs including VSMCs and pericytes in adult humans, it is intriguing to observe an impaired barrier function in BMECs that carry a *NOTCH3* variant. It is possible that the *NOTCH3* expression is higher in BMECs than in the peripheral ECs, which has not been documented previously. We then compared the *NOTCH3* mRNA levels between the iPSC-BMECs and iPSC-ECs. Indeed, the results showed that *NOTCH3* expression in BMECs was about 2-fold higher than that of ECs (Figure 5A), while Claudin 5 was highly expressed in BMECs compared to ECs (Figure 5B). The higher expression of *NOTCH3* in BMECs than in the peripheral ECs suggests a possible role of *NOTCH3* in the brain endothelial cells, which requires further study in the future.

3.3. iPSC-derived wild-type MCs, astrocytes and neurons fail to rescue the impaired barrier function of CADASIL iPSC-BMECs

Given the fact that the BBB barrier function of BMECs can be significantly enhanced by MCs, astrocytes and neurons (Figure 2), it is interesting to know if the damaged BBB function of the CADASIL BMECs could be rescued by these neurovascular cell types. Thus, the CADASIL iPSC-BMECs were co-cultured with wild type iPSC-derived MCs, astrocytes and neurons, respectively,

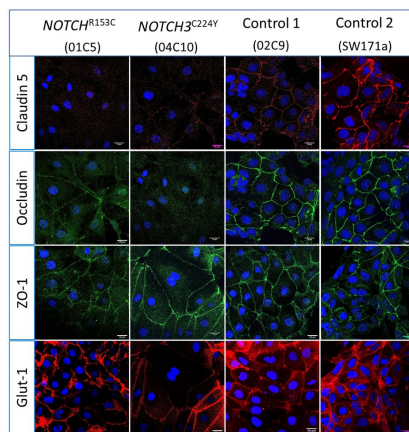


FIGURE 4

Immunostaining of tight junction proteins and glucose transporter protein in Cerebral Autosomal Dominant Arteriopathy with Subcortical Infarcts and Leukoencephalopathy (CADASIL) induced pluripotent stem cell (iPSC) derived brain microvascular endothelial-like cells (BMECs). iPSCs from CADASIL patients carrying *NOTCH3* variants R153C and C224Y, respectively, were differentiated into BMECs and immunofluorescently stained for tight junction proteins Claudin 5, Occludin, and ZO-1, and glucose transporter Glut-1. Images were acquired using a confocal microscope. Scale bar, 20 μm .

and the TEER was recorded as described above. Data showed that the TEER of CADASIL iPSC-BMECs could not be rescued by the wild-type iPSC derived MCs (Figures 6A, B). Astrocytes and neurons seemed to be able to slightly increase the TEER of the mutant BMECs with statistical significances; however, such function was significantly blunted compared to the co-culture of these cells with the wild-type BMECs (Figures 6C–F). These results suggest intrinsic damage in BMEC BBB function in CADASIL patients.

4. Discussion

Using iPSCs from CADASIL patients, we established an *in vitro* NVU model and demonstrated a reduced BBB barrier function in the CADASIL iPSC-BMECs (Figures 1, 3), which could not be rescued, or sufficiently rescued, by co-culture with other neurovascular cell types including MCs, astrocytes and neurons that were derived from wild types iPSCs (Figure 6). Furthermore, the CADASIL iPSC-MCs completely failed to enhance the barrier function of the wild type BMECs (Figures 6A, B). Our findings provide new insight into the molecular mechanisms for the most common genetic small vessel disease, CADASIL.

Cerebral Autosomal Dominant Arteriopathy with Subcortical Infarcts and Leukoencephalopathy is a late-onset condition with recurrent ischemic strokes starting at an average age of 45 years. However, some non-specific symptoms like migraine can appear as early as the teens with abnormal MRI changes, before the onset of strokes. The impaired neurovascular interactions we demonstrated from the iPSC CADASIL model could at least partially explain the early CADASIL pathologies in the brain. It is likely that the impaired neurovascular interaction could render the brain

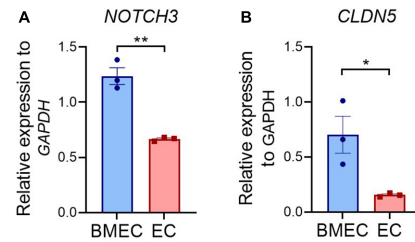


FIGURE 5

Comparison of *NOTCH3* expression between induced pluripotent stem cell (iPSC) derived brain microvascular endothelial-like cells (BMECs) and endothelial cells (ECs). Wild-type iPSCs differentiated into BMECs and peripheral ECs. The expression of *NOTCH3* (A) and *CLDN5* (B) were determined using quantitative real time polymerase chain reaction (qRT-PCR). Data are presented as mean \pm SEM. Student's *t*-test, * $p < 0.05$, ** $p < 0.001$, $n = 3$.

vulnerable to the subsequent stroke episodes, which accelerates the disease progression to cognitive impairment and dementia.

The unique barrier properties of the brain ECs are not predetermined but induced by the neuronal cues during brain development (Janzer and Raff, 1987; Alvarez et al., 2013; Daneman and Prat, 2015). The complex neurovascular interactions are important for proper BBB function, however, it is challenging to directly measure the contribution of each individual neurovascular cell type to the BBB function in *in vivo* animal models. In this regard, the iPSC model provides a feasible solution. By co-culturing the iPSC-derived neurovascular cell types in different combinations with the iPSC-BMECs, our iPSC model recapitulated the previous understanding that astrocytes, MCs and neurons could all independently enhance the BBB barrier function of the BMECs and have a synergistic effect (Figure 2; Daneman and Prat, 2015).

During early embryonic development, vascular sprouts interact with the emergent pericytes and radial glial cells in the parenchyma, establishing the initial tight junctions and the immature BBB phenotype (Daneman et al., 2009, 2010b; Liebner et al., 2011). The development and maturation of the BBB continue during late stages of embryonic development and postnatally when astrocytes becoming a more abundant cell type in the parenchyma. Astrocytes secrete a range of factors including TGF- β , glial-derived neurotrophic factor (GDNF), FGF2, angiopoietin 1 (ANG1), sonic hedgehog (Shh), and retinoic acid (RA), all of which induce the formation of and strengthen the tight junctions of BMECs (Alvarez et al., 2013). Indeed, our results demonstrated a most effective influence of astrocytes in enhancing the TEER value of BMECs comparing to that of the MCs and neurons (Figure 2C). However, we found that the TEER of the CADASIL iPSC-BMECs could only be slightly rescued by the wild-type iPSC-astrocytes or iPSC-neurons, which is in great contrast to the significant enhancement of TEER in wild-type iPSC-BMECs by the wild-type iPSC-astrocytes and neurons (Figures 6C–F). This suggested intrinsic defects of BMECs in CADASIL.

Pericytes are another critical player in the maturation and maintenance of the BBB (Armulik et al., 2011; Brown et al., 2019). However, it was found that pericytes do not necessarily induce the BBB *per se* but are important in the prevention of the “leaky” properties possibly by inhibiting transcytosis and the expression of leukocyte adhesion molecules (LAMs) on ECs

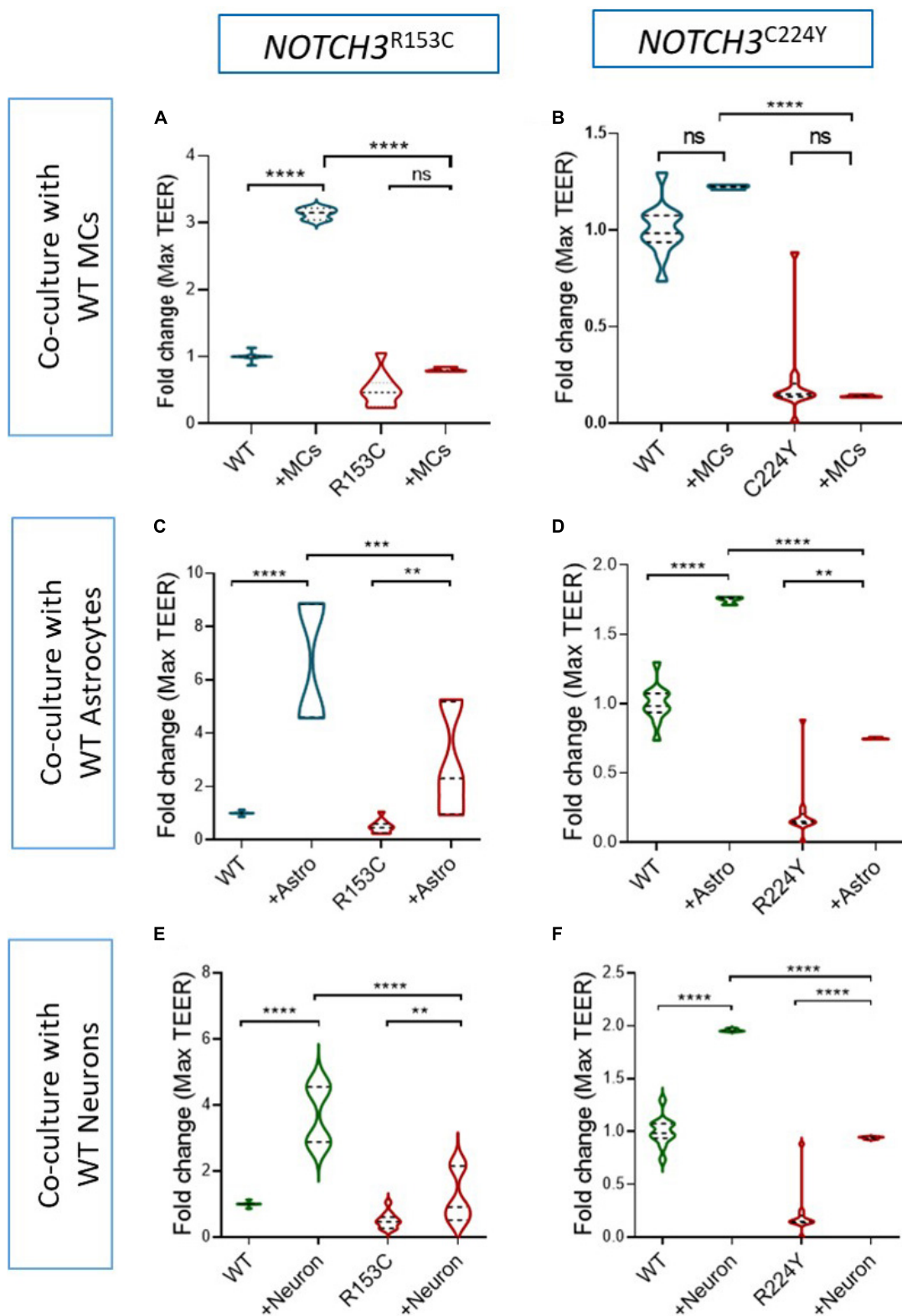


FIGURE 6

Effect of wild-type induced pluripotent stem cell (iPSC)-derived mural cells (MCs), astrocytes and neurons on the barrier function of Cerebral Autosomal Dominant Arteriopathy with Subcortical Infarcts and Leukoencephalopathy (CADASIL) iPSC-brain microvascular endothelial-like cells (BMECs). **(A)** CADASIL or wild-type (WT) control iPSC derived BMECs were seeded on the insert of Transwell and co-cultured with the WT iPSC derived MCs **(A,B)**, astrocytes **(C,D)**, and neurons **(E,F)** that were grown on the bottom of the Transwell plate. Transendothelial electrical resistance (TEER) was measured for five consecutive days. The maximum TEER were compared. iPSC lines from two CADASIL patients (*NOTCH3*^{R153C} and *NOTCH3*^{R244Y}) are presented in the figure. Data are mean ± SEM, *n* = 3. Two-way ANOVA with Tukey's *post-hoc* test, ***p* < 0.01, ****p* < 0.001, and *****p* < 0.0001, *n* = 3.

(Armulik et al., 2010, 2011; Daneman et al., 2010b; Daneman and Prat, 2015). We found that the wild-type iPSC-MCs significantly upregulated the TEER of the wild-type iPSC-BMECs, but the CADASIL iPSC-MCs failed to upregulate the TEER formed by iPSC-BMECs (Figures 2D–G). Although we have not determined the effect of the CADASIL iPSC-MCs on the transcytosis of BMECs, our previous work found that the CADASIL iPSC-MC is the primary driver to destabilize the microvascular network by a reduced expression of PDGFR β , decreased secretion of VEGF, and inducing apoptosis of the adjacent ECs (Kelleher et al., 2019). It is plausible that the failure of the CADASIL iPSC-MCs to upregulate the BBB function of wild-type iPSC-BMECs could be at least partially due to a damaging effect of the CADASIL iPSC-MCs on the iPSC-BMECs, and this cannot be reversed by factors from unaffected iPSC-MCs.

NOTCH3 is considered to be predominantly expressed in the arterial VSMCs and pericytes (Chabriat et al., 2020). However, we found that the BBB function was significantly reduced in the iPSC-BMECs that carry the CADASIL *NOTCH3* variants (Figure 3). The results were confirmed by using iPSC lines from two CADASIL patients on multiple independent experiments. The unique properties of the BMECs that distinguish them from the peripheral ECs led us to explore if *NOTCH3* is more important in BMECs than in the peripheral ECs. Using qRT-PCR we indeed found a significantly higher expression of *NOTCH3* in the iPSC-BMECs than in the iPSC-ECs, suggesting a likely unique function of *NOTCH3* in BMECs. In a pilot study, we also knocked down *NOTCH3* in iPSC-BMECs using siRNA and the initial data demonstrated a reduced TEER value in the *NOTCH3*-knockdown iPSC-BMECs, which implicates a role of *NOTCH3* on the BBB barrier function, although additional work is required to support this conclusion. Interestingly, a recent publication by Dabertrand et al. (2021) demonstrated a reduced Kir2.1 activity in cerebral capillary endothelial cells, but not in arteriolar endothelial cells in a CADASIL mouse model, which was due to compromised PIP₂ synthesis in the capillary ECs, suggesting the involvement of BMECs in CADASIL pathology. However, to conclude a definite link between the CADASIL *NOTCH3* variants and BMEC function, more work is required in the future.

In summary, we have demonstrated an impaired neurovascular interaction that contributes to a reduced BBB function in the CADASIL iPSC model. The findings contribute to our current knowledge of the molecular mechanisms underlying CADASIL pathologies and shed light on the understanding of the CNS phenotypes resulting from vascular dysfunction in SVD. Further study is required to refine molecular mechanisms underlying the impaired neurovascular interaction and functional damage of the BBB in CADASIL and identify therapeutic targets. The iPSCs derived from CADASIL patients, albeit an *in vitro* model, is a valuable complement to the *in vivo* animal models and represent a useful human model system for the study of SVD.

4.1. Limitations

Our study has limitations. Firstly, the iPSC control lines were derived from healthy individuals, rather than isogenic controls. Therefore, the observed phenotypes caused by the *NOTCH3*

variants may be influenced by variation between individuals. To minimize this effect, we have used iPSC lines from three healthy individuals to compare with two patient iPSC lines in different combinations. It would be ideal to replicate the work using isogenic control lines in the future. Secondly, the protocol of iPSC-BMECs differentiation we adapted (Lippmann et al., 2011, 2020; Stebbins et al., 2016) may produce cells that have epithelial properties as argued by a recent publication (Lu et al., 2021). Although we detected CD31 and VE-Cadherin in the iPSC-BMECs which represent endothelial properties, the angiogenic capacity was not as good as that of the peripheral ECs. We acknowledge the challenge to produce true BMECs that have both endothelial properties and a high BBB function. Effort should be made to further improve the BMEC differentiation protocol in the future.

Data availability statement

The original contributions presented in this study are included in the article/Supplementary material, further inquiries can be directed to the corresponding author.

Author contributions

WZ designed and carried out most of the experiments and data analysis. XZ carried out experiments and conducted most of data analysis. XQ carried out experiments. SK provided iPSC lines and edited manuscript. NH supervised project, assisted with study design, and edited manuscript. TW supervised and designed the project, data interpretation, and manuscript writing. All authors contributed to the article and approved the submitted version.

Funding

This work was funded by a Medical Research Council (MC_PC_16033 Momentum Award for Dementia), Alzheimer's Research UK Manchester and North West Network Centre Fund, and a Project Grant from British Heart Foundation (Grant No.: PG/12/31/29527). WZ was funded by the China Scholarship Council—University of Manchester postgraduate joint scholarship award.

Acknowledgments

We thank the University of Manchester Bioimaging Core Facility for guidance on confocal microscopy and sample preparation. We thank Pankaj Sharma from Institute of Cardiovascular Research, Royal Holloway, University of London, Imperial College London, and Helen Murphy and Iris Trender-Gerhard from Manchester Centre for Genomic Medicine (MCGM) for helping recruiting CADASIL patients, which contribute to the establishment of the CADASIL iPSC lines. We thank Adam Dickinson for establishing the CADASIL iPSC lines and control lines, and Steven Woods for creating the SW171a and SW174a lines.

Conflict of interest

The authors declare that the research was conducted in the absence of any commercial or financial relationships that could be construed as a potential conflict of interest.

Publisher's note

All claims expressed in this article are solely those of the authors and do not necessarily represent those of their affiliated

organizations, or those of the publisher, the editors and the reviewers. Any product that may be evaluated in this article, or claim that may be made by its manufacturer, is not guaranteed or endorsed by the publisher.

Supplementary material

The Supplementary Material for this article can be found online at: <https://www.frontiersin.org/articles/10.3389/fncel.2023.1195470/full#supplementary-material>

References

- Abbott, N. J., Ronnback, L., and Hansson, E. (2006). Astrocyte-endothelial interactions at the blood-brain barrier. *Nat. Rev. Neurosci.* 7, 41–53. doi: 10.1038/nrn1824
- Adib-Samii, P., Brice, G., Martin, R. J., and Markus, H. S. (2010). Clinical spectrum of CADASIL and the effect of cardiovascular risk factors on phenotype: Study in 200 consecutively recruited individuals. *Stroke* 41, 630–634. doi: 10.1161/STROKEAHA.109.568402
- Alvarez, J. I., Katayama, T., and Prat, A. (2013). Glial influence on the blood brain barrier. *Glia* 61, 1939–1958. doi: 10.1002/glia.22575
- Andreone, B. J., Lacoste, B., and Gu, C. (2015). Neuronal and vascular interactions. *Annu. Rev. Neurosci.* 38, 25–46. doi: 10.1146/annurev-neuro-071714-033835
- Armulik, A., Genove, G., and Betsholtz, C. (2011). Pericytes: Developmental, physiological, and pathological perspectives, problems, and promises. *Dev. Cell* 21, 193–215. doi: 10.1016/j.devcel.2011.07.001
- Armulik, A., Genove, G., Mae, M., Nisancioglu, M. H., Wallgard, E., Niaudet, C., et al. (2010). Pericytes regulate the blood-brain barrier. *Nature* 468, 557–561. doi: 10.1038/nature09522
- Brown, L. S., Foster, C. G., Courtney, J. M., King, N. E., Howells, D. W., and Sutherland, B. A. (2019). Pericytes and neurovascular function in the healthy and diseased brain. *Front. Cell Neurosci.* 13:282. doi: 10.3389/fncel.2019.00282
- Chabriat, H., Joutel, A., Dichgans, M., Tournier-Lasserre, E., and Boussier, M. G. (2009). CADASIL. *Lancet Neurol.* 8, 643–653. doi: 10.1016/S1474-4422(09)70127-9
- Chabriat, H., Joutel, A., Tournier-Lasserre, E., and Boussier, M. G. (2020). CADASIL: Yesterday, today, tomorrow. *Eur. J. Neurol.* 27, 1588–1595. doi: 10.1111/ene.14293
- Chai, A. B., Callaghan, R., and Gelissen, I. C. (2022). Regulation of P-Glycoprotein in the brain. *Int. J. Mol. Sci.* 23:14667. doi: 10.3390/ijms232314667
- Charlton, R. A., Morris, R. G., Nitkunan, A., and Markus, H. S. (2006). The cognitive profiles of CADASIL and sporadic small vessel disease. *Neurology* 66, 1523–1526. doi: 10.1212/01.wnl.0000216270.02610.7e
- Coomer, B. L., and Stewart, P. A. (1985). Morphometric analysis of CNS microvascular endothelium. *Microvasc. Res.* 30, 99–115. doi: 10.1016/0026-2862(85)90042-1
- Dabertrand, F., Harraz, O. F., Koide, M., Longden, T. A., Rosehart, A. C., Hill-Eubanks, D. C., et al. (2021). PIP₂ corrects cerebral blood flow deficits in small vessel disease by rescuing capillary Kir2.1 activity. *Proc. Natl. Acad. Sci. U.S.A.* 118:e2025998118. doi: 10.1073/pnas.2025998118
- Daneman, R., Agalliu, D., Zhou, L., Kuhnert, F., Kuo, C. J., and Barres, B. A. (2009). Wnt/beta-catenin signaling is required for CNS, but not non-CNS, angiogenesis. *Proc. Natl. Acad. Sci. U.S.A.* 106, 641–646. doi: 10.1073/pnas.0805165106
- Daneman, R., and Prat, A. (2015). The blood-brain barrier. *Cold Spring Harb. Perspect. Biol.* 7:a020412. doi: 10.1101/cshperspect.a020412
- Daneman, R., Zhou, L., Agalliu, D., Cahoy, J. D., Kauschal, A., and Barres, B. A. (2010a). The mouse blood-brain barrier transcriptome: A new resource for understanding the development and function of brain endothelial cells. *PLoS One* 5:e13741. doi: 10.1371/journal.pone.0013741
- Daneman, R., Zhou, L., Kebede, A. A., and Barres, B. A. (2010b). Pericytes are required for blood-brain barrier integrity during embryogenesis. *Nature* 468, 562–566. doi: 10.1038/nature09513
- Desmond, D. W., Moroney, J. T., Lynch, T., Chan, S., Chin, S. S., and Mohr, J. P. (1999). The natural history of CADASIL: A pooled analysis of previously published cases. *Stroke* 30, 1230–1233. doi: 10.1161/01.str.30.6.1230
- Hongjin, W., Han, C., Baoxiang, J., Shiqi, Y., and Xiaoyu, X. (2020). Reconstituting neurovascular unit based on the close relations between neural stem cells and endothelial cells: An effective method to explore neurogenesis and angiogenesis. *Rev. Neurosci.* 31, 143–159. doi: 10.1515/revneuro-2019-0023
- Janzer, R. C., and Raff, M. C. (1987). Astrocytes induce blood-brain barrier properties in endothelial cells. *Nature* 325, 253–257. doi: 10.038/325253a0
- Jarosz-Griffiths, H. H., Corbett, N. J., Rowland, H. A., Fisher, K., Jones, A. C., Baron, J., et al. (2019). Proteolytic shedding of the prion protein via activation of metalloproteinase Adam10 reduces cellular binding and toxicity of amyloid-beta oligomers. *J. Biol. Chem.* 294, 7085–7097. doi: 10.1074/jbc.RA118.005364
- Joutel, A., Corpechot, C., Ducros, A., Vahedi, K., Chabriat, H., Mouton, P., et al. (1996). Notch3 mutations in CADASIL, a hereditary adult-onset condition causing stroke and dementia. *Nature* 383, 707–710.
- Joutel, A., Favrole, P., Labauge, P., Chabriat, H., Lescoat, C., Andreux, F., et al. (2001). Skin biopsy immunostaining with a Notch3 monoclonal antibody for CADASIL diagnosis. *Lancet* 358, 2049–2051.
- Joutel, A., Vahedi, K., Corpechot, C., Troesch, A., Chabriat, H., Vayssiere, C., et al. (1997). Strong clustering and stereotyped nature of Notch3 mutations in CADASIL patients. *Lancet* 350, 1511–1515. doi: 10.1016/S0140-6736(97)08083-5
- Kelleher, J., Dickinson, A., Cain, S., Hu, Y., Bates, N., Harvey, A., et al. (2019). Patient-specific iPSC model of a genetic vascular dementia syndrome reveals failure of mural cells to stabilize capillary structures. *Stem Cell Rep.* 13, 817–831. doi: 10.1016/j.stemcr.2019.10.004
- Liebner, S., Czupalla, C. J., and Wolburg, H. (2011). Current concepts of blood-brain barrier development. *Int. J. Dev. Biol.* 55, 467–476.
- Lippmann, E. S., Al-Ahmad, A., Azarin, S. M., Palecek, S. P., and Shusta, E. V. (2014). A retinoic acid-enhanced, multicellular human blood-brain barrier model derived from stem cell sources. *Sci. Rep.* 4:4160. doi: 10.1038/srep04160
- Lippmann, E. S., Azarin, S. M., Kay, J. E., Nessler, R. A., Wilson, H. K., Al-Ahmad, A., et al. (2012). Derivation of blood-brain barrier endothelial cells from human pluripotent stem cells. *Nat. Biotechnol.* 30, 783–791.
- Lippmann, E. S., Azarin, S. M., Palecek, S. P., and Shusta, E. V. (2020). Commentary on human pluripotent stem cell-based blood-brain barrier models. *Fluids Barriers CNS* 17:64. doi: 10.1186/s12987-020-00222-3
- Lippmann, E. S., Weidenfeller, C., Svendsen, C. N., and Shusta, E. V. (2011). Blood-brain barrier modeling with co-cultured neural progenitor cell-derived astrocytes and neurons. *J. Neurochem.* 119, 507–520. doi: 10.1111/j.1471-4159.2011.07434.x
- Lu, T. M., Houghton, S., Magdeldin, T., Duran, J. G. B., Minotti, A. P., Snead, A., et al. (2021). Pluripotent stem cell-derived epithelium misidentified as brain microvascular endothelium requires ETS factors to acquire vascular fate. *Proc. Natl. Acad. Sci. U.S.A.* 118:e2016950118. doi: 10.1073/pnas.2016950118
- Narayan, S. K., Gorman, G., Kalara, R. N., Ford, G. A., and Chinnery, P. F. (2012). The minimum prevalence of CADASIL in northeast England. *Neurology* 78, 1025–1027. doi: 10.1212/WNL.0b013e31824d586c
- Neal, E. H., Marinelli, N. A., Shi, Y., McClatchey, P. M., Balotin, K. M., Gullett, D. R., et al. (2019). A simplified, fully defined differentiation scheme for producing blood-brain barrier endothelial cells from human iPSCs. *Stem Cell Rep.* 12, 1380–1388. doi: 10.1016/j.stemcr.2019.05.008
- Newman, K., Argyriou, A., and Wang, T. (2020). "Induced pluripotent stem cell modeling of genetic small vessel disease," in *Recent advances in iPSC disease modeling*, ed. A. Birbrair (Amsterdam: Elsevier), 131–159. doi: 10.1016/B978-0-12-822227-0.00007-7
- Pfaffl, M. W. (2001). A new mathematical model for relative quantification in real-time RT-PCR. *Nucleic Acids Res.* 29:e45. doi: 10.1093/nar/29.9.e45

- Pulido, R. S., Munji, R. N., Chan, T. C., Quirk, C. R., Weiner, G. A., Weger, B. D., et al. (2020). Neuronal activity regulates blood-brain barrier efflux transport through endothelial circadian genes. *Neuron* 108, 937–952.e7. doi: 10.1016/j.neuron.2020.09.002
- Razvi, S. S., Davidson, R., Bone, I., and Muir, K. W. (2005). The prevalence of cerebral autosomal dominant arteriopathy with subcortical infarcts and leucoencephalopathy (CADASIL) in the west of Scotland. *J. Neurol. Neurosurg. Psychiatry* 76, 739–741. doi: 10.1136/jnnp.2004.051847
- Rutten, J. W., Dauwerse, H. G., Gravesteyn, G., Van Belzen, M. J., Van Der Grond, J., Polke, J. M., et al. (2016). Archetypal NOTCH3 mutations frequent in public exome: Implications for CADASIL. *Ann. Clin. Transl. Neurol.* 3, 844–853. doi: 10.1002/acn3.344
- Sharma, P., Wang, T., Brown, M. J., and Schapira, A. H. (2001). Fits and strokes. *Lancet* 358:120. doi: 10.1016/S0140-6736(01)05331-4
- Shi, Y., Kirwan, P., and Livesey, F. J. (2012). Directed differentiation of human pluripotent stem cells to cerebral cortex neurons and neural networks. *Nat. Protoc.* 7, 1836–1846. doi: 10.1038/nprot.2012.116
- Stebbins, M. J., Wilson, H. K., Canfield, S. G., Qian, T., Palecek, S. P., and Shusta, E. V. (2016). Differentiation and characterization of human pluripotent stem cell-derived brain microvascular endothelial cells. *Methods* 101, 93–102. doi: 10.1016/j.ymeth.2015.10.016
- Tata, M., and Ruhrberg, C. (2018). Cross-talk between blood vessels and neural progenitors in the developing brain. *Neuronal Signal* 2:NS20170139.
- Wallez, Y., and Huber, P. (2008). Endothelial adherens and tight junctions in vascular homeostasis, inflammation and angiogenesis. *Biochim. Biophys. Acta* 1778, 794–809.
- Wang, T., Holt, C. M., Xu, C., Ridley, C., Jones, R. P. O., Baron, M., et al. (2007). Notch3 activation modulates cell growth behaviour and cross-talk to Wnt/TCF signalling pathway. *Cell Signal* 19, 2458–2467. doi: 10.1016/j.cellsig.2007.07.019
- Wood, K. A., Rowlands, C. F., Thomas, H. B., Woods, S., O'flaherty, J., Douzgou, S., et al. (2020). Modelling the developmental spliceosomal craniofacial disorder Burn-McKeown syndrome using induced pluripotent stem cells. *PLoS One* 15:e0233582. doi: 10.1371/journal.pone.0233582
- Woods, S., Bates, N., Dunn, S. L., Serracino-Inglott, F., Hardingham, T. E., and Kimber, S. J. (2020). Generation of human-induced pluripotent stem cells from anterior cruciate ligament. *J. Orthop. Res.* 38, 92–104.
- Yazdani, S., Jaldin-Fincati, J. R., Pereira, R. V. S., and Klip, A. (2019). Endothelial cell barriers: Transport of molecules between blood and tissues. *Traffic* 20, 390–403.